

Neutron-induced fission cross section of ^{234}U measured at the CERN n_TOF facility

D. Karadimos,^{1,2,*} R. Vlastou,¹ K. Ioannidis,² P. Demetriou,^{3,4} M. Diakaki,¹ V. Vlachoudis,⁵ P. Pavlopoulos,⁶ V. Konovalov,⁷ U. Abbondando,⁸ G. Aerts,⁹ H. Álvarez,¹⁰ F. Alvarez-Velarde,¹¹ S. Andriamonje,⁹ J. Andrzejewski,¹² P. Assimakopoulos,^{2,†} L. Audouin,¹³ G. Badurek,¹⁴ P. Baumann,¹⁵ F. Bečvář,¹⁶ E. Berthoumieux,⁹ F. Calviño,¹⁷ D. Cano-Ott,¹¹ R. Capote,¹⁸ A. Carrillo de Albornoz,¹⁹ V. Chepel,²⁰ E. Chiaveri,⁵ N. Colonna,²¹ G. Cortes,¹⁷ A. Couture,²² J. Cox,²² S. David,¹³ R. Dolfini,²³ C. Domingo-Pardo,²⁴ A. Dorochenko,²⁵ W. Dridi,⁹ I. Duran,¹⁰ Ch. Eleftheriadis,²⁶ M. Embid-Segura,¹¹ L. Ferrant,^{27,‡} A. Ferrari,⁵ R. Ferreira-Marques,²⁰ L. Fitzpatrick,⁵ H. Fraiss-Koelbl,²⁸ K. Fuji,²¹ W. Furman,⁷ I. Goncalves,¹⁹ R. Gallino,²⁹ P. Cennini,⁵ E. Gonzalez-Romero,¹¹ A. Goverdovski,²⁵ F. Gramegna,³⁰ E. Griesmayer,²⁸ C. Guerrero,¹¹ F. Gunsing,⁹ B. Haas,³¹ R. Haight,³² M. Heil,³³ A. Herrera-Martinez,⁵ M. Igashira,³⁴ S. Isaev,¹³ E. Jericha,³⁵ Y. Kadi,⁵ F. Käppeler,³³ D. Karamanis,² M. Kerveno,¹⁵ V. Ketlerov,²⁵ P. Koehler,³⁶ D. Kolokolov,²⁵ M. Krstička,¹⁶ C. Lamboudis,²⁶ H. Leeb,³⁵ A. Lindote,²⁰ I. Lopes,²⁰ M. Lozano,¹⁸ S. Lukic,¹⁵ J. Marganić,¹² L. Marques,¹⁹ S. Marrone,²¹ C. Massimi,³⁷ P. Mastinu,³⁰ A. Mengoni,⁵ P. M. Milazzo,⁸ C. Moreau,⁸ M. Mosconi,³³ F. Neves,²⁰ H. Oberhummer,¹⁴ S. O'Brien,²² M. Oshima,³⁸ J. Pancin,⁹ C. Papadopoulos,¹ C. Paradela,¹⁰ N. Patronis,² A. Pavlik,¹⁴ L. Perrot,⁹ R. Plag,³³ A. Plompen,³⁹ A. Plukis,⁹ A. Poch,¹⁷ C. Pretel,¹⁷ J. Quesada,¹⁸ T. Rauscher,⁴⁰ R. Reifarh,³² M. Rosetti,⁴¹ C. Rubbia,²³ G. Rudolf,¹⁵ P. Rullhusen,³⁹ J. Salgado,¹⁹ L. Sarchiapone,⁵ I. Savvidis,²⁶ M. Sedysheva,⁷ K. Stamoulis,² C. Stephan,¹³ G. Tagliente,²¹ J. L. Tain,²⁴ L. Tassan-Got,¹³ L. Tavora,¹⁹ R. Terlizzi,²¹ A. Tsinganis,¹ G. Vannini,³⁷ P. Vaz,¹⁹ A. Ventura,⁴¹ D. Villamarin,¹¹ M. C. Vincente,¹¹ F. Voss,³³ H. Wendler,⁵ M. Wiescher,²² and K. Wisshak³³

(n_TOF Collaboration)

¹National Technical University of Athens, Greece²University of Ioannina, Greece³NCSR Demokritos, Athens, Greece⁴Nuclear Data Section, International Atomic Energy Agency, A-1400 Vienna, Austria⁵CERN, Geneva, Switzerland⁶Pôle Universitaire Léonard de Vinci, Paris La Défense, France⁷Joint Institute for Nuclear Research, Frank Laboratory of Neutron Physics, Dubna, Russia⁸Istituto Nazionale di Fisica Nucleare, Trieste, Italy⁹CEA/Saclay - DSM, Gif-sur-Yvette, France¹⁰Universidad de Santiago de Compostela, Spain¹¹Centro de Investigaciones Energeticas Medioambientales y Technologicas, Madrid, Spain¹²University of Lodz, Lodz, Poland¹³Centre National de la Recherche Scientifique/IN2P3 - IPN, Orsay, France¹⁴Institut für Isotopenforschung und Kernphysik, Universität Wien, Austria¹⁵Centre National de la Recherche Scientifique/IN2P3 - IReS, Strasbourg, France¹⁶Charles University, Prague, Czech Republic¹⁷Universitat Politècnica de Catalunya, Barcelona, Spain¹⁸Universidad de Sevilla, Spain¹⁹Instituto Tecnológico e Nuclear, Lisbon, Portugal²⁰LIP - Coimbra & Departamento de Física da Universidade de Coimbra, Portugal²¹Istituto Nazionale di Fisica Nucleare, Bari, Italy²²University of Notre Dame, Notre Dame, Indiana, USA²³Università degli Studi Pavia, Pavia, Italy²⁴Consejo Superior de Investigaciones Científicas - University of Valencia, Spain²⁵Institute of Physics and Power Engineering, Kaluga region, Obninsk, Russia²⁶Aristotle University of Thessaloniki, Greece²⁷Centre National de la Recherche Scientifique IN2P3 - IPN, Orsay, France²⁸Fachhochschule Wiener Neustadt, Wiener Neustadt, Austria²⁹Dipartimento di Fisica Generale, Università di Torino and Sezione INFN di Torino, I-10125 Torino, Italy³⁰Laboratori Nazionali di Legnaro, Italy³¹Centre National de la Recherche Scientifique/IN2P3 - CENBG, Bordeaux, France³²Los Alamos National Laboratory, New Mexico, USA³³Karlsruhe Institut of Technology, Campus Nord, Institut für Kernphysik, Germany³⁴Tokyo Institute of Technology, Tokyo, Japan³⁵Atominstytut der Österreichischen Universitäten, Technische Universität Wien³⁶Oak Ridge National Laboratory, Physics Division, Oak Ridge, Tennessee, USA³⁷Dipartimento di Fisica, Università di Bologna, and Sezione INFN di Bologna, Italy³⁸Japan Atomic Energy Research Institute, Tokai-mura, Japan³⁹CEC-JRC-IRMM, Geel, Belgium

⁴⁰*Department of Physics and Astronomy - University of Basel, Basel, Switzerland*⁴¹*ENEA, Bologna, Italy*

(Received 21 December 2013; published 15 April 2014)

The neutron-induced fission cross section of ²³⁴U has been measured at the CERN n_TOF facility relative to the standard fission cross section of ²³⁵U from 20 keV to 1.4 MeV and of ²³⁸U from 1.4 to 200 MeV. A fast ionization chamber (FIC) was used as a fission fragment detector with a detection efficiency of no less than 97%. The high instantaneous flux and the low background characterizing the n_TOF facility resulted in wide-energy-range data (0.02 to 200 MeV), with high energy resolution, high statistics, and systematic uncertainties below 3%. Previous investigations around the energy of the fission threshold revealed structures attributed to β -vibrational levels, which have been confirmed by the present measurements. Theoretical calculations have been performed, employing the TALYS code with model parameters tuned to fairly reproduce the experimental data.

DOI: [10.1103/PhysRevC.89.044606](https://doi.org/10.1103/PhysRevC.89.044606)

PACS number(s): 25.85.Ec, 28.65.+a, 27.90.+b, 24.75.+i

I. INTRODUCTION

Neutron-induced reactions on minor actinides are of considerable importance in various fields of both fundamental and applied nuclear physics. The phenomena that are governed by the structured fission barrier result in new information on the forces operating in highly deformed many-body systems. The main applications are related to novel nuclear technologies for nuclear waste transmutation as well as to the future production of clean and safe nuclear energy. The available experimental data present many discrepancies and cannot be considered as a reliable basis for practical applications and for testing nuclear models [1]. Therefore, more accurate and self-consistent experimental data are needed to increase the predictive power of phenomenological models and to improve the systematic development of model parameters.

Among minor actinides, ²³⁴U is included in the priority list suggested by the IAEA [2] since it plays an important role in the Th-U fuel cycle which is proposed to replace the Pu-U cycle in advanced generation-IV reactors and in subcritical accelerator driven systems (ADSs). Experimental fission data on ²³⁴U(*n, f*) from the n_TOF facility have recently been published in a wide energy range, from 1 eV to 1 GeV, implementing parallel plate avalanche counters (PPACs) for the detection of fission fragments [3]. These measurements constitute the first set of data that cover such a wide energy range with an uncertainty of about 4%. Earlier data, published in a wide energy region near and above threshold, have been measured by Lamphere in the range 136 keV to 4.05 MeV, by Lowry from 300 keV to 1.5 MeV, by White *et al.* from 40 keV to 14.1 MeV, by James *et al.* from a few eV to 8.9 MeV, by Meadows in the range 0.6 to 14.7 MeV, and by Manabe *et al.* from 13.5 to 14.9 MeV [4–12].

Cross-section ratios relative to ²³⁵U have also been measured by Behrens and Carlson from 0.1 to 30 MeV, by Kanda *et al.* from 0.5 to 7 MeV, by Goverdovskiy *et al.* from 5 to 10 MeV, by Lisowski *et al.* from 0.6 to 395 MeV, and by Fursov *et al.* from 0.13 to 7.4 MeV [13–17].

Discrepancies of more than 10% at certain energies among these data necessitate new measurements, taking advantage of the recent availability of new state-of-the-art neutron facilities with advanced detection and acquisition systems. In the present work, the ²³⁴U(*n, f*) cross section has been measured at the CERN n_TOF [18] facility with respect to ²³⁵U and ²³⁸U fission cross sections by using the fast ionization chamber (FIC) [19].

This work constitutes part of an extensive program of fission cross-section measurements that have been performed and are still in progress at the n_TOF facility and data deduced from this measurement campaign are compared with the data from literature and mainly with the n_TOF data obtained by using the PPAC detector system [3]. The data are also compared with theoretical predictions obtained by means of the TALYS code [20].

II. EXPERIMENTAL METHOD

A. Neutron beam

The n_TOF facility has provided the means for high-resolution time-of-flight measurements of capture and fission reactions since 2002. Neutrons are generated via high-energy proton-induced spallation reactions on a massive lead target surrounded by a 5.8-cm-thick layer of cooling water. The high intensity of the proton bunches (7×10^{12} protons per bunch), the short pulse width (16 ns), and the low duty cycle (1 pulse per 2.4 s) provided by the CERN Proton Synchrotron (PS), along with the long flight path for the produced neutrons (182.5 m), make a unique neutron TOF facility for high-resolution cross-section measurements in an energy range from thermal to GeV neutrons. The spallation neutrons are accompanied by an intense flash of γ rays and ultrarelativistic particles, suppressed by appropriate shielding, a 1.5 T sweeping magnet, and two collimators at 137 and 176 m from the lead target. The second collimator, with an aperture of 8 cm diameter, defines the neutron beam profile for fission measurements. The neutron beam line is extended for an additional 12 m beyond the experimental area to minimize the effect of back-scattered neutrons. The neutron energy is determined via their time of flight (TOF) by using the γ flash from the impact of the proton bunch on the lead target as the start time reference.

*dkaradim@gmail.com

†Deceased

TABLE I. Average surface density and mass values of the targets, obtained by alpha-spectroscopy along with their isotopic impurities. For ^{234}U and ^{238}U , 14 and 2 targets, respectively, were used and the average values are reported in the table.

Target	Target nominal isotope			Target contamination	
	Specific activity (Bq/mg)	Mass (mg)	Average surface density (atoms/cm ²)	Isotope	Mass (mg)
^{234}U	$230\,252 \pm 60$	2.87 ± 0.06	390 ± 50	^{232}U	$1.52 \times 10^{-5} \pm 0.02 \times 10^{-5}$
^{238}U	12.44 ± 0.01	9.46 ± 0.12	1117 ± 94		
^{235}U	79.98 ± 0.06	4.69 ± 0.06	626 ± 84	^{234}U	$8.8 \times 10^{-5} \pm .6 \times 10^{-5}$

B. Targets

The uranium oxide (U_3O_8) targets were thin layers of isotopically pure materials deposited in the form of a 5.2-cm-diameter disk on a 100- μm -thick Al backing by using the painting technique. The samples were provided by the Institute of Physics and Power Engineering, Obninsk, and the Joint Institute of Nuclear Research, Dubna. Their homogeneity, mass, and possible contamination were determined by using CR-39 solid state nuclear track detectors, alpha-spectroscopy, and Rutherford back scattering (RBS) techniques.

The alpha-spectroscopy measurements were carried out using two Si surface barrier detectors of 50 and 3000 mm² active surfaces in order to combine good resolution and good statistics, respectively. The high purity of all targets was verified from all the tests. The ^{234}U and ^{235}U targets were found to contain negligible contamination of ^{232}U and ^{234}U , respectively, as revealed by the alpha-peaks provided by the daughter isotopes of their decay chains [21]. The total mass and isotopic impurities of the targets are presented in Table I.

The surface density at various points has been determined with use of the Rutherford backscattering spectrometry (RBS) technique, with an external proton beam of 2 MeV and 1 mm diameter, delivered by the 5.5 MV Van de Graaff accelerator of the Institute of Nuclear Physics at the NCSR ‘‘Demokritos.’’ For each target, 5 to 10 points were measured and the RBS spectra were analyzed with the SIMNRA code [22], while for the normalization factor the Al backing counts were considered. The analysis of the various points on the targets showed that there is no symmetry in the deposition of the material on the target around the center of the disk and that the targets were homogeneous within 15%. The average values of the surface density for each target are shown in Table I. FLUKA [23,24] simulations for the neutron beam profile with the fission collimation (8 cm) revealed that the beam above 20 keV (which is the lower limit of the present data) it is almost flat in the region of the sample. Thus, any nonuniformities are not important in the case of fission measurements in the energy region of interest.

The targets were additionally characterized for their homogeneity with the use of CR-39 detectors. The detectors were placed on top of the samples for a few seconds to a few hours, depending on the activity of the sample, in order to achieve a surface-track concentration of at least 200 tracks/mm². The detectors were etched in a 6 N aqueous NaOH solution, maintained at 75 °C. Images of the detectors’ surfaces were captured with the use of a setup including a microscope, a video camera, a frame grabber, and computer recording software. The tracks were counted using the TRIACK II code [25]. The

homogeneity of the sample has been estimated to be of the order of 15%.

C. Detector and data acquisition

The measurements were performed with a FIC developed by the Institute of Physics and Power Engineering, Obninsk, in collaboration with the Joint Institute of Nuclear Research, Dubna, and the EET group at CERN [19]. The setup is composed of 17 ionization chambers stacked together in a cylindrical stainless-steel chamber 50 cm in length, thus allowing the simultaneous measurement on several isotopes. Each chamber consists of a 100- μm -thick central Al cathode plated on both sides with the fissile material and two 15- μm -thick Al anodes at 10 mm from the cathode. The electrodes were 12 cm in diameter, while the diameter of the deposited target material was 5.2 cm. Seven ^{234}U targets were mounted inside the FIC detector along with one ^{235}U and one ^{238}U reference target. Three off-beam positions have also been used to account for the neutron background effects as well as one dummy (empty) target mounted in beam to record background events. The distance between the spallation target and the first sample in the FIC detector was 185.6 m. The detector setup operated as a sealed ionization chamber with a gas mixture of 90% pure Ar and 10% CF_4 at a pressure of 720 mbar. The 10 mm distance between electrodes was sufficient to produce much higher signals than the ones from the alpha particles coming from the decay of the targets and the competing neutron-induced reactions. MCNPX [26] simulations indicated that the neutron-flux attenuation in the Al electrodes and windows is of the order of a few per thousand in the energy region of interest [19].

The fission events were detected by means of the energy deposited in the gas by the fission fragments and the detector signals were amplified by an AD844 current feedback operational amplifier and digitized with 4 CAEN-V767 FADC (flash analog-to-digital converter) at a sampling rate of 40 MHz and 3 multihit time discriminators (TDCs) CAEN-V767 modules. The FADC recorded the signal in a time window of 100 μs and the TDC inside a 200 ms time window which for a 185 m flight path corresponds to neutron energy down to 18 keV and 4 meV, respectively. The trigger used for the modules was the PS signal (arrival of a proton pulse). The digitized signal was stored on a local PC and later transferred to the CERN Central Advanced STORAGE System (CASTOR) for subsequent offline analysis.

The ^{238}U , a dummy target, and seven ^{234}U targets were connected to both FADC and TDC channels independently.

For the ^{235}U target hardware, a zero-suppression algorithm was applied to the connected FADC channel, making it possible to record fission signals induced by thermal neutrons. For this reason, the TDC channel connected to the ^{235}U target was used for triggering the FADC, which was recording 5 presamples and 10 postsamples at each trigger, i.e., 5 bins before and 10 bins after the signal that triggered the TDC [27].

D. Data analysis

The FADC data were analyzed using pulse shape analysis techniques to distinguish between fission and background events. The analysis technique and the code which has been developed for this purpose are described in detail in Ref. [28].

The main issue to be addressed was the rippling and undershooting of the baseline in the FADC output caused by the γ flash, which is significant in the early phase of the FADC sequence, as can be seen in Fig. 1. These effects follow the same pattern in all FADC outputs, thus allowing us to estimate an “average” signal, which was then subtracted from the original raw signal, considerably reducing the background, while the fission events remain unaffected. At some points, however the signal identification was impossible due to the strong fluctuations of the signal induced by the γ flash. Thus, for the neutron-energy range above 200 MeV it was found impossible to extract reliable cross section values. A typical example of the pulse shape analysis procedure from the raw data to the final fit of fission fragments is demonstrated in Fig. 1.

The pulse shape analysis of the fission events was performed by fitting the signals with an exponential expression [28] using the MINUIT code [29], providing the time and amplitude for each detector signal. This pulse shape analysis

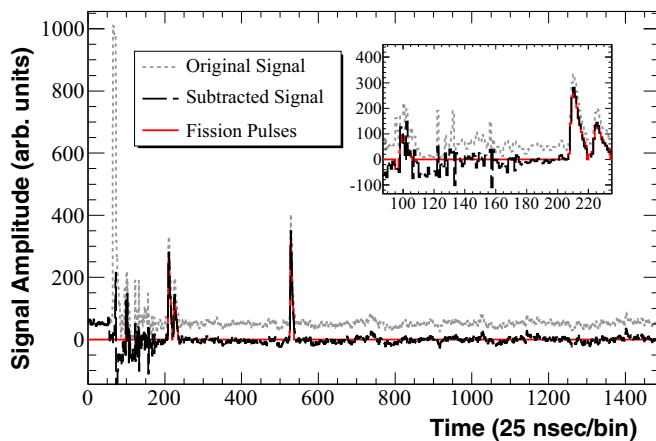


FIG. 1. (Color online) Typical FADC content for one of the ^{234}U channels. The full detector signal has been recorded for 4096×25 ns while in the figure only the 1500 first bins are shown. The inset illustrates the early phase of the sequence in the energy range down to 30 MeV approximately, where the undershooting and rippling of the detector baseline caused by the γ flash can be observed (dotted, gray), as well as the recovery of the baseline after the “average” subtraction (dashed, black). The first peak in the original signal represents the γ flash and the following peaks correspond to fission fragments (solid, red).

technique takes full advantage of the excellent time resolution of the n_TOF setup, achieving resolving times of the order of the FADC unit (25 ns), leading to negligible dead-time effects. The amplitude distribution of the pulses from the ^{234}U reference samples and dummy target can then be deduced, as shown in Fig. 2. The amplitude distributions were then fit with three exponential functions shown as dotted lines in Fig. 2. The first curve represented low-amplitude background events, while the other two described fission events. The overall fit plotted as solid line reproduced very well the experimental amplitude distribution (dashed line) of all isotopes, as can be seen in Fig. 2.

The discrimination of fission from background events has been achieved by applying a threshold to the signal-amplitude distributions. The value used in this analysis is 100 FADC units (Fig. 2). The criterion for setting this value is to minimize the counts from the “dummy” amplitude distribution [Fig. 2(a)] while keeping the maximum fission counts from the target [(Figs. 2(b)–2(d)]. Nevertheless, the threshold applied to reject the background events affected the number of real fission events. Thus, a correction factor ϵ has been estimated from the overlapping tails of the three curves and its uncertainty has been extracted from the fitting parameter errors. The deduced values for each target are shown in Table II. The residual alpha-particle background was estimated from runs without the neutron beam and was found to be negligible [30].

The neutron energy associated with each fission event was deduced from its time of flight, which is defined by the time between the arrival of the prompt γ flash and the detection of the fission signal. For the precise determination of the neutron flight distance, the geometrical length has been corrected for the distance covered in the lead target and the coolant and moderator water layer. The distance correction has been evaluated as a function of neutron energy by means of Monte Carlo simulations [31]. The uncertainty in the neutron energy determination depends on the accuracy of the fitting and is much less than the energy binning used to deduce the cross section (20 to 200 bins/decade) and is of the order of 10^{-2} to 10^{-4} , depending on the energy region. Specifically, the logarithmic binning of the histograms for the energy range 20 keV to 0.9 MeV was set to 200 bins per decade (bpd), from 0.9 to 1.4 MeV to 20 bpd, from 1.4 to 15 MeV to 50 bpd and for 15 to 200 MeV to 20 bpd.

The fission cross section was calculated from the ratio of the reaction rate histograms by means of the expression

$$\sigma_X(E) = C \frac{S_X(E)}{S_R(E)} \sigma_R(E), \quad C = \frac{A_X m_R \epsilon_X}{A_R m_X \epsilon_R}, \quad (1)$$

where X stands for the nucleus we measure and R for the ^{235}U or ^{238}U reference nucleus, for which the neutron-induced fission cross section is well known. With A and m we denote the atomic number and the mass and with S the number of events measured. The factor ϵ is the correction due to the threshold applied to each FADC channel and the values used are presented in Table II. The number of events S has been corrected for losses of fission fragments due to the self absorption in the target material. This effect has been estimated from detailed FLUKA simulations. An external routine was developed in order to create fission fragments based on the

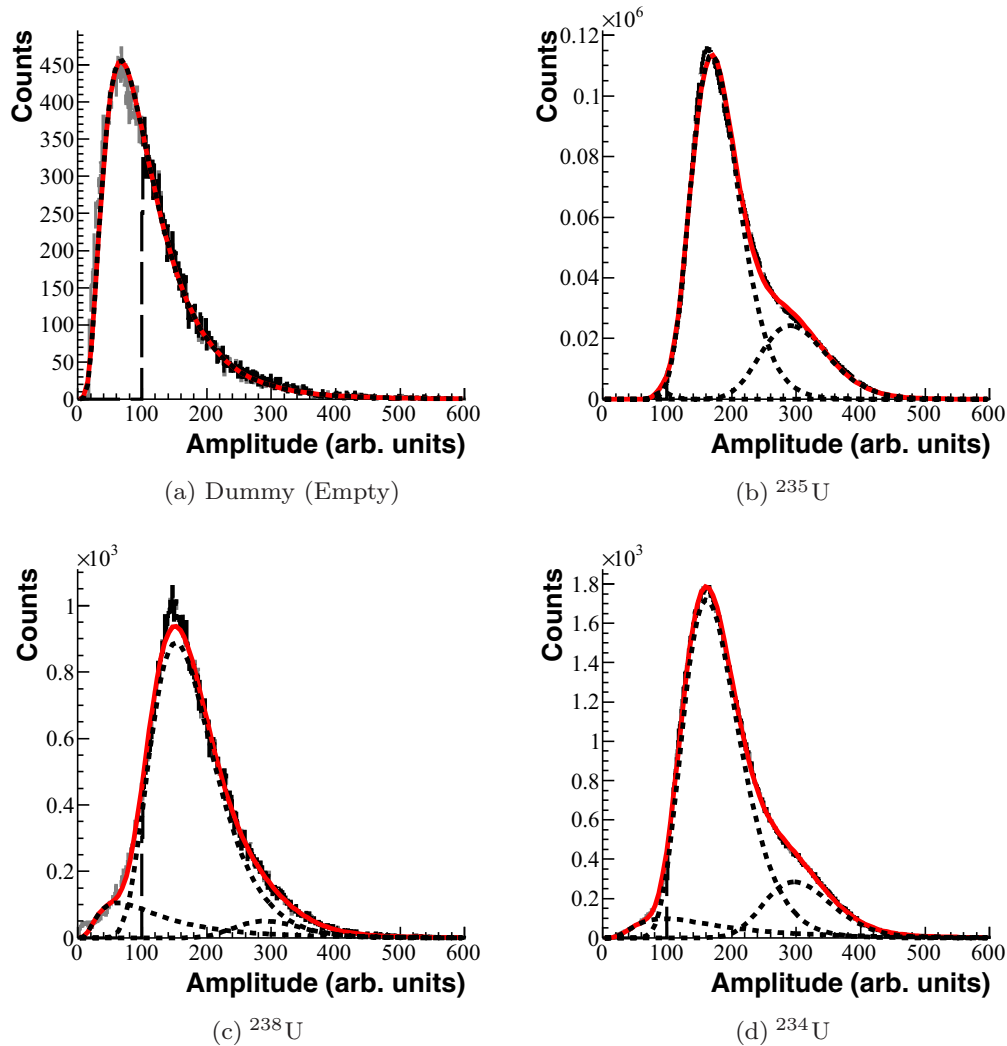


FIG. 2. (Color online) Amplitude distribution. The dotted lines represent the exponential fitting functions and the solid red line is the overall fit. The vertical line represents the threshold applied at 100 FADC units.

systematics of Ref. [32], which were isotropically distributed in the volume of each target and their energy deposition was scored in the gas of the FIC detector. The percentage of the fission fragments exiting the target material was 98.8% for ^{234}U , 96.5% for ^{238}U , and 98.0% for ^{235}U .

Due to the fact that the ^{235}U FADC channel was triggered by the TDC, dead time effects were observed for the ^{235}U fission fragments. In order to account for this effect, the $^{234}\text{U}(n, f)$ cross section deduced with respect to the $^{235}\text{U}(n, f)$ reference reaction was normalized to the $^{234}\text{U}(n, f)$ cross section with

respect to $^{238}\text{U}(n, f)$ in the region 0.9 to 1.4 MeV, where both reference reactions overlap with fair statistics for ^{238}U and acquisition reliability for ^{235}U . The $^{234}\text{U}(n, f)$ cross section was derived relative to the $^{235}\text{U}(n, f)$ reaction in the energy region 200 keV to 1 MeV, where the $^{238}\text{U}(n, f)$ reaction cannot be used due to its low cross section, while from 1.4 to 200 MeV the ^{238}U fission cross section was used. The cross sections for the two reference reactions have been taken from the Evaluated Nuclear Database recommended by IAEA [33] as standards.

The main sources of systematic uncertainties are related to the sample masses, the normalization to the reference-reaction cross section, and the correction factor for the threshold applied to the data. The systematic uncertainties in the sample mass determination are presented in Table I and vary from 1.2% to 2%. The uncertainty of the normalization procedure corresponds to that of the fission cross section for ^{235}U and ^{238}U which are typically 2% in the energy region under study. The uncertainty in the correction factor ϵ is of the order of 1-2%, as reported in Table II. Thus, the overall systematic uncertainties remain below 3%. The statistical uncertainties

TABLE II. Correction factors ϵ for threshold applied to amplitude spectrum of each sample.

Target	Correction factor ϵ
^{235}U	1.00 ± 0.01
^{238}U	0.98 ± 0.02
^{234}U	0.97 ± 0.01

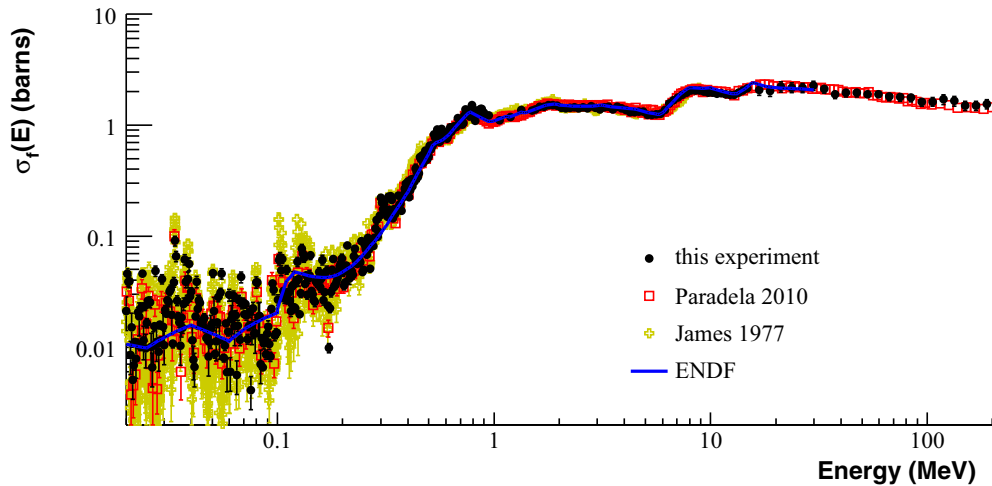


FIG. 3. (Color online) Fission cross section of ^{234}U from 20 keV to 200 MeV. The present n_TOF data are compared with ENDF [34] and with selected experimental data [3,9]. The error bars of the present data correspond to the statistical uncertainties.

are shown along with the cross-section data and are of the order of 8% in the region 20 to 900 keV, 7% in the region 0.9 to 1 MeV, and 5% from 10 to 200 MeV.

III. RESULTS AND DISCUSSION

The results for the ^{234}U fission cross section from 20 keV to 200 MeV are presented in Fig. 3 along with data by James *et al.* [9] and Paradela *et al.* [3] as well as the ENDF values [34]. An overall agreement within the limits of their experimental errors can be observed. In more detail, in the energy region from 20 keV to 1.4 MeV, the measured cross-section data are shown in Fig. 4 along with the available data from the literature [3,5–7,9–11]. The energy binning up to 0.9 MeV was kept as high as possible (200 bins/decade) in an attempt to achieve an adequate energy resolution to compare the present results with those of James *et al.* The energy binning of the data by James *et al.* is still 3 to 4 times finer. Nevertheless, the structures

observed by James *et al.* below the fission threshold are largely confirmed by the present data, as can be seen in Figs. 5–9 presenting in detail the energy regions 15–40 keV, 40–100 keV, 100–180 keV, 180–400 keV, and 400–900 keV, respectively. Some discrepancies observed in Fig. 7 could be attributed to the deterioration of the resolution with increasing energy compared to the fine width of the structures in the 100–180 keV energy region, thus smearing out some maxima observed by James *et al.* From the evaluated data only the JEFF [35] ones consider some of these resonance-like structures, while the ENDF [34] and JENDL [36] data provide an average value in the subthreshold-energy region. The present data confirm also the plateaus at 310, 550, and 770 keV, which were observed by James *et al.* and attributed to β -vibrational levels in the second minimum of the fission barrier. From 0.9 to 1.4 MeV the energy binning was 20 bins per decade, due to the low statistics of the ^{238}U fission events in this energy region. In the region 1.4 to 15 MeV presented in Fig. 10, the data by James *et al.* [9],

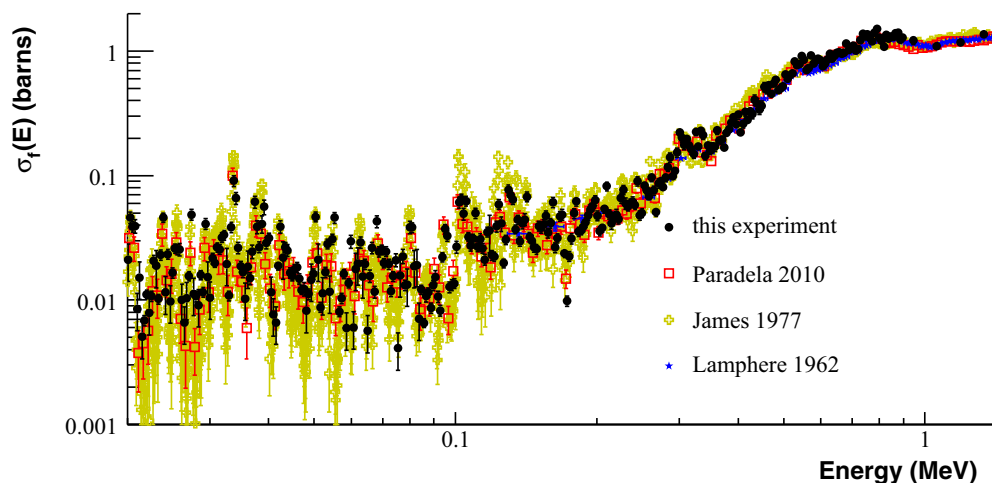


FIG. 4. (Color online) The fission cross section of ^{234}U from 20 keV to 1.4 MeV (200 bins per decade up to 0.9 MeV and 20 bins per decade between 0.9 and 1.4 MeV) compared with previous measurements [3,5,9]. The data of Lowry, White, and Meadows [6,8,10] are also in good agreement with the present data, but they are not shown in the figure for reasons of clarity. ^{235}U was used as reference in this energy region.

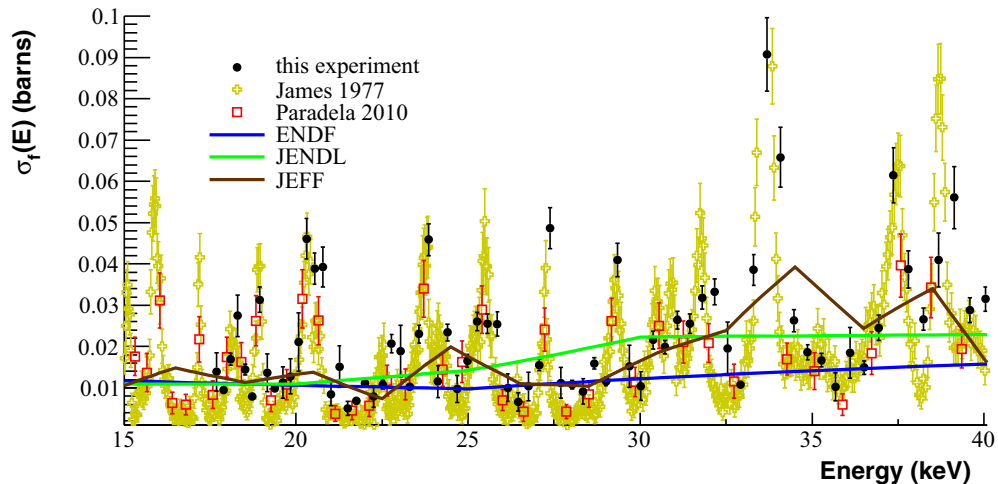


FIG. 5. (Color online) Fission cross section of ^{234}U from 15 to 40 keV compared with the ENDF, JEFF, and JENDL databases as well as with previous measurements.

Paradela *et al.* [3], Manabe *et al.* [12], Meadows [11], White [8], and Lamphere [5] are in reasonable agreement within the limits of their experimental errors, while the data of Ref. [9] exhibit some maxima and minima compared to the more smooth behavior revealed by the rest of the measurements. At the plateau of the first-chance fission up to 6 MeV the present data agree with all the other data within their experimental errors. In the region of the second-chance fission threshold, between 6 and 8 MeV, the data by Meadows [10] are higher than those of James *et al.* by 15%, while the data by Paradela *et al.* lie between them. The present data agree with those by Paradela *et al.* within their uncertainties. Above 10 MeV, only the data by Manabe and Paradela *et al.* exist in literature and they seem to be in good agreement with the present data. In this energy region, in order to achieve reasonable statistics, the energy binning was 50 bins per decade. Above 15 MeV and up to 200 MeV the present data are shown in Fig. 11 along with the data by Paradela *et al.* and are seen to be in a reasonable agreement. In this high-energy region, due to the low intensity

of the neutron beam, the binning was decreased to 20 bins per decade.

IV. NUCLEAR MODEL CALCULATIONS

The measured cross sections were also compared with calculations performed with the TALYS nuclear reaction code [20]. The TALYS code incorporates several nuclear reaction models to describe the nuclear reaction mechanisms competing in the energy region ranging from a few keV to 200 MeV. The nuclear structure information used by TALYS is taken from state-of-the-art nuclear structure libraries [37]. In practice, fission is described as a decay channel of the formed compound nucleus (CN) and is calculated within the Hauser-Feshbach theory. It therefore depends on the transmission coefficients which describe the probability of tunneling through the fission barrier, and the nuclear level density (NLD) corresponding to the density of levels on top of the fission barrier (saddle points). The fission barriers are

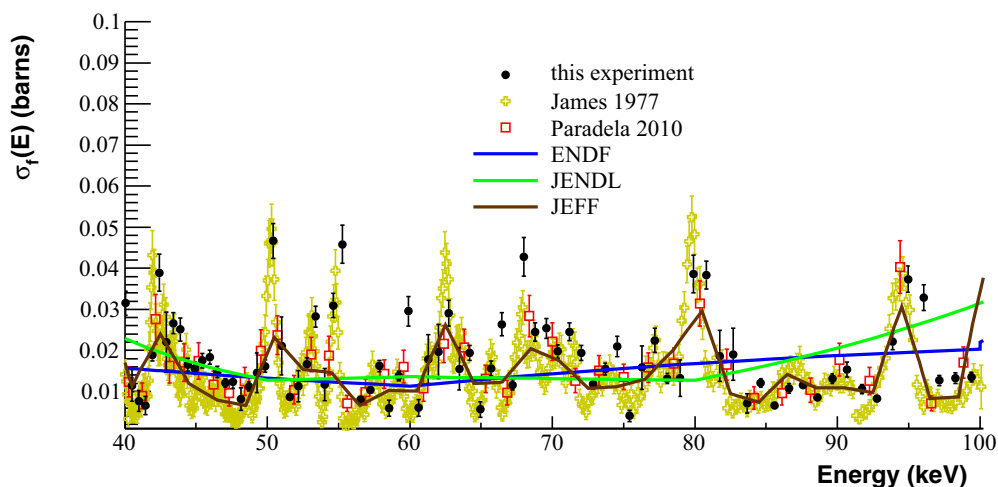


FIG. 6. (Color online) Fission cross section of ^{234}U from 40 to 100 keV compared with ENDF, JEFF, and JENDL databases as well as with previous measurements.

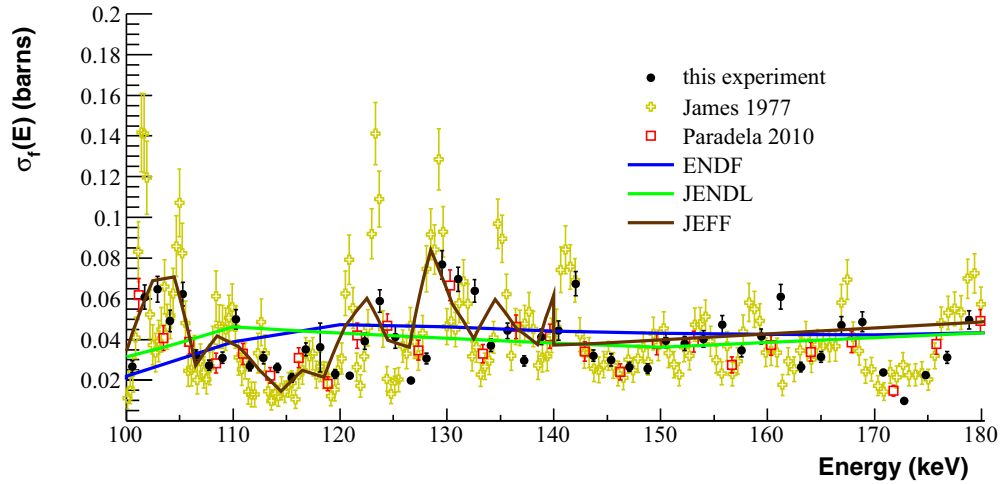


FIG. 7. (Color online) Fission cross section of ^{234}U from 100 to 180 keV compared with ENDF, JEFF, and JENDL databases as well as with previous measurements.

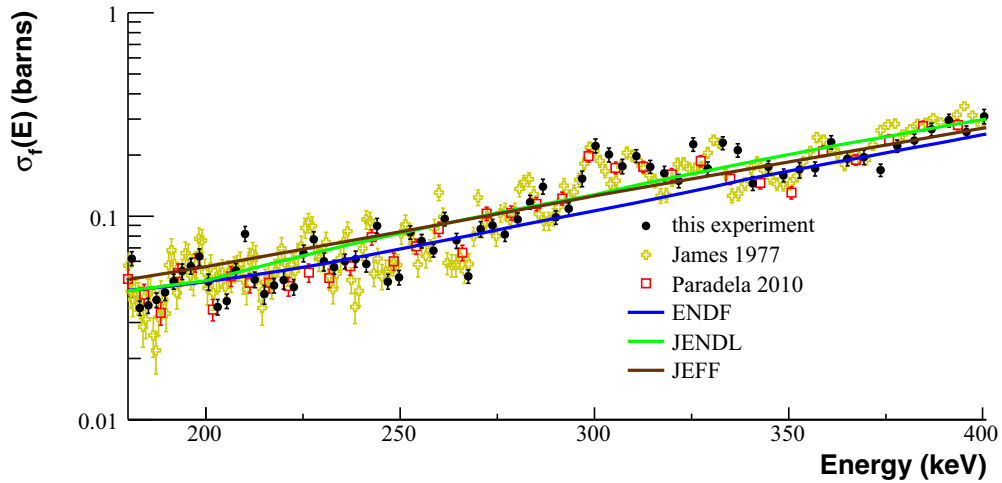


FIG. 8. (Color online) Fission cross section of ^{234}U from 180 to 400 keV compared with ENDF, JEFF, and JENDL databases as well as with previous measurements.

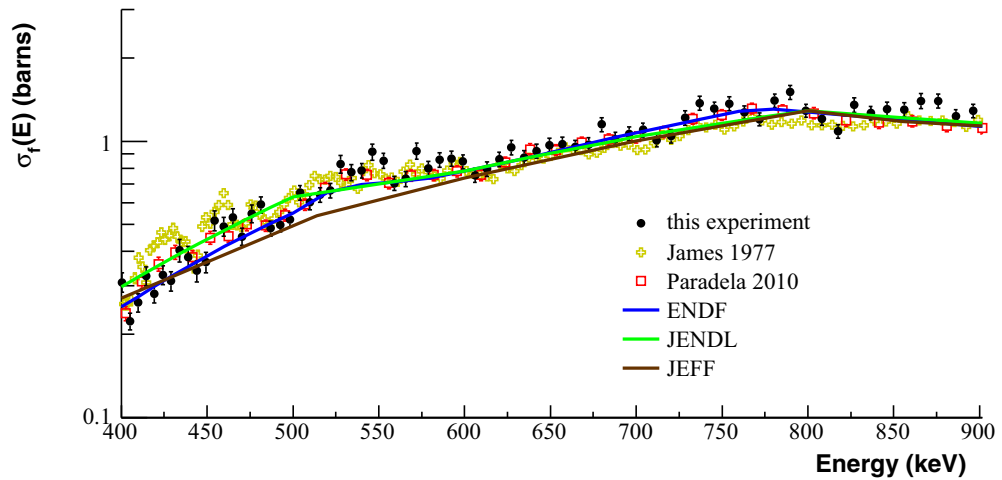


FIG. 9. (Color online) Fission cross section of ^{234}U from 400 to 900 keV compared with ENDF, JEFF, and JENDL databases as well as with previous measurements.

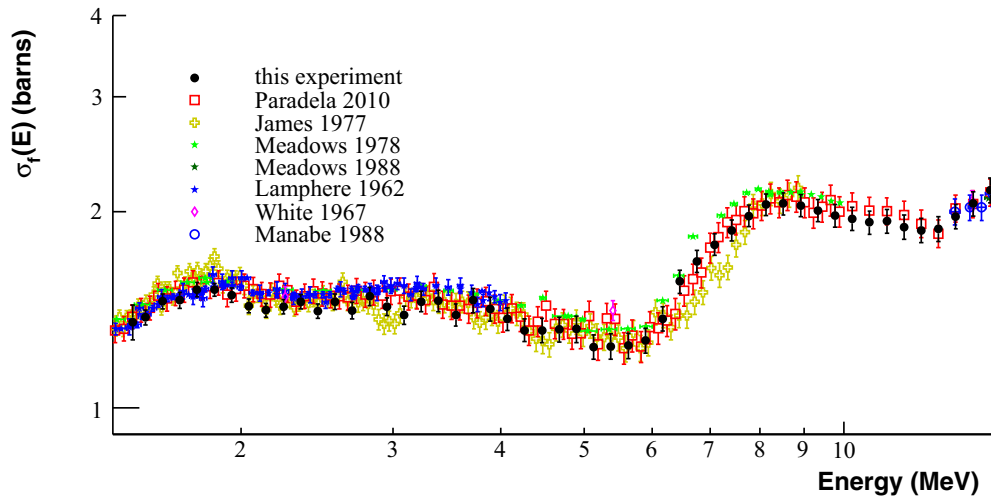


FIG. 10. (Color online) Fission cross section of ^{234}U from 1.4 to 5 MeV (50 bins per decade) and 5 to 15 MeV (20 bins per decade), compared with previous measurements [3,5,7,9–12]. ^{238}U was used as reference in this energy region.

described by a succession of alternating parabolic wells and humps, which form a two- or three-humped barrier. In the limit of full dumping of vibrational excitations in the wells, the barrier becomes equivalent to a set of two or three decoupled humps, whose heights (B_f) and widths ($\hbar\omega$) are provided by models or are extracted from experimental cross sections.

Within this simplistic approach and using the default values for all the input parameters such as optical potential [38], fission barrier heights and widths [37], ground-state and saddle-point level densities [20], we obtain the solid line shown in Fig. 12. Note that Maslov's [37] compilation of empirical barrier parameters includes only a few of the minor and major actinide isotopes. In the absence of any empirical values, TALYS uses the predictions of the rotational liquid drop model [39].

As can be seen from Fig. 12, the default calculations underestimate the slope of the subthreshold fission cross sections in the 0.1–1 MeV energy range. They also fail to describe the first-, second- and third-chance fission plateaus

and slopes and, furthermore, they seriously underestimate the multichance fission cross sections in the higher-energy region from 30 up to 200 MeV. This failure is clearly a result of the crude approximations that are made in the simplistic approach and also of the inadequacy of the global input parameters used. In an attempt to improve the comparison with the data, the height B_f of the outer fission barrier of ^{235}U was reduced by 2% and the width $\hbar\omega$ was increased by 10%. This adjustment enhanced the subthreshold tail below 0.1 MeV and improved the slope of the excitation function between 0.1 and 1 MeV. Furthermore, by increasing the ground-state level density parameters a_n of ^{235}U and ^{234}U by 3% and 18%, respectively, the first-chance and second-chance fission cross sections in the plateaus were reduced. In addition, the sudden dips between the plateaus and thresholds were smoothed out in agreement with the data. The significant enhancement of the fission cross section in the high-energy region, from 30 to 200 MeV, was achieved by replacing the barrier parameters of Ref. [39] with

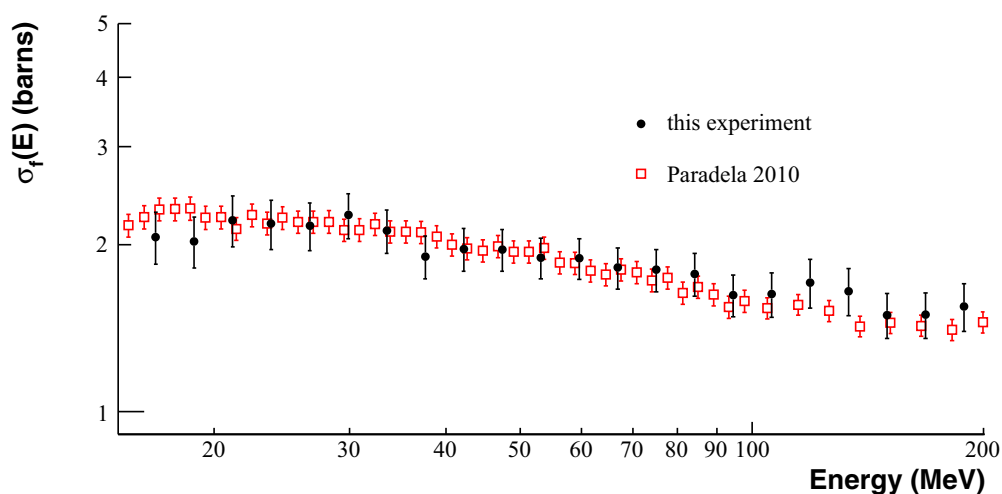


FIG. 11. (Color online) The fission cross section of ^{234}U from 15 to 200 MeV (20 bins per decade), compared with the only available data by Paradela. ^{238}U was used as reference in this energy region.

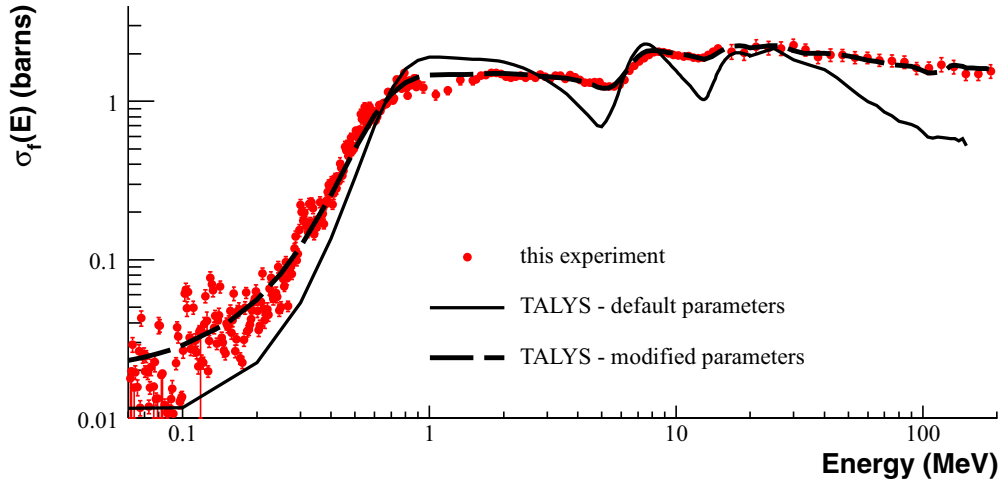


FIG. 12. (Color online) Fission cross section of ^{234}U from this experiment versus TALYS calculations with default (solid line) and modified parameters (dashed line).

those obtained from the finite-range droplet model [40] for those nuclides not included in Maslov's compilation.

The effect of these modifications on the other neutron-induced reaction channels such as (n, xn) has not been investigated in detail; however, a comparison of the (n, n') cross sections, before and after the modifications, showed that, in the case of ^{235}U where a lot of measured data are available, the (n, n') cross sections are enhanced by 20% with respect to the data [41] and 15% with respect to the default TALYS cross sections. For ^{234}U , the effect on the (n, n') cross sections is more pronounced; however, in this case there are no measured data to compare with. Ideally, one would aim at obtaining one set of fitted parameters that would consistently reproduce all the open neutron-induced reaction channels. However, such a task requires a more thorough theoretical investigation, which is clearly beyond the scope of this paper.

The improved fission cross sections, shown in Fig. 12 by the dashed line, are able to reproduce on average the experimental data, over the whole energy range. However, they are still unable to describe the structure that is observed in the subthreshold energy region from 0.3 to 0.6 MeV, as well as the resolved peak observed at around 1 MeV just below the top of the barrier. These structures are attributed to resonant states in the isomeric fission wells, which are completely neglected in these calculations. In fact, the fine structure mentioned above can only be explained by considering a triple-humped barrier for ^{235}U , with resonant states in the first (class II) and second isomeric wells (class III). As has been shown in similar cases [42], in a partial damping model approach, the resonant structure in the isomeric wells is only partially damped and therefore leads to the appearance of fine structure in the fission cross sections at energies below the top of the barrier. The fine structure observed in the subthreshold region from 0.3 to 0.6 MeV arises from partial damping of resonant class-II states, while the structure observed at around 0.8 to 1 MeV is attributable to resonant class-III states in the second isomeric well.

Because the formalism developed in Ref. [42] has already been implemented in the nuclear reaction code EMPIRE [43], it is planned to use this code to study the fine structure in

the low-energy region. A detailed theoretical study of the $^{234}\text{U}(n, f)$ channel, with proper consideration of the structure properties of the nucleus with increasing deformation, such as triple-humped barriers and resonant states, as well as the effects due to other competing reaction channels, will be the subject of a future presentation.

V. SUMMARY AND CONCLUSIONS

The $^{234}\text{U}(n, f)$ cross section has been studied for neutron energies from 20 keV to 200 MeV at the CERN n_TOF facility. Fission fragments from thin high-purity samples were counted in a fast ionization chamber (FIC). The output of the detector electrodes were connected to both TDC (CAEN V767) and FADC (CAEN V676) modules and the digitized signal was stored for further offline analysis. Pulse-shape analysis techniques have been applied for the analysis of the FADC data in order to distinguish fission from background events. The ripple and undershoot of the baseline in the FADC output were eliminated by subtracting an "average" signal from the actual data. The extracted cross section values are compared with previous measurements and are found to be in reasonable agreement.

Calculations of $^{234}\text{U}(n, f)$ were performed with the TALYS code assuming a double-humped fission barrier for ^{235}U and neglecting the effect of resonant states in the isomeric wells. With some further parameter adjustment, within this simplistic approach we were able to describe the average features of the fission cross sections over the entire energy region. However, the fine structure observed in the subthreshold energy regions 0.3 to 0.6 MeV and 0.8 to 1 MeV, could not be reproduced as it requires a more sophisticated approach that assumes a triple-humped fission barrier for ^{235}U and takes due consideration of the resonant class-II and class-III states lying in the first and second isomeric wells, respectively.

ACKNOWLEDGMENT

Financial support from the Greek State Fellowship Foundation is gratefully acknowledged.

- [1] A. Fessler, A. Plompen, D. Smith, J. Meadows, and Y. Ikeda, *Nucl. Sci. Eng.* **134**, 171 (2000).
- [2] A. Plompen and A. Mengoni, *Summary Report of Consultants Meeting on Minor Actinide Nuclear Reaction Data (MANREAD)* (IAEA-NDS, Vienna, 2007), pp. INDC(NDS)-0512.
- [3] C. Paradela *et al.*, *Phys. Rev. C* **82**, 034601 (2010).
- [4] R. Lamphere, *Phys. Rev.* **91**, 655 (1953).
- [5] R. Lamphere, *Nucl. Phys.* **38**, 561 (1962).
- [6] L. Lowry, *Tech. Rep.* (Los Alamos National Laboratory, 1954).
- [7] P. White and G. Warner, *J. Nucl. Energy* **21**, 671 (1967).
- [8] P. White, J. Hodgkinson, and G. Wall, in *Proc. Conf. on Physics and Chemistry of Fission* (IAEA, Salzburg, Austria, 1964), pp. EANDC(UK)535.
- [9] G. James, J. Dabbs, J. Harvey, N. Hill, and R. Schindler, *Phys. Rev. C* **15**, 2083 (1977).
- [10] J. Meadows, *Nucl. Sci. Eng.* **65**, 171 (1978).
- [11] J. Meadows, *Ann. Nucl. Energy* **15**, 421 (1988).
- [12] F. Manabe, K. Kanda, T. Iwasaki, H. Terayama, Y. Karino, M. Baba, and N. Hirakawa, *Tech. Rep.* **52**, 97 (1988).
- [13] J. Behrens and G. Carlson, *Nucl. Sci. Eng.* **63**, 250 (1977).
- [14] K. Kanda, H. Imaruoka, K. Yoshida, O. Sato, and N. Hirakawa, *Radiat. Eff.* **93**, 233 (1986).
- [15] A. Goverdovskiy, A. Gordyushin, B. Kuzminov, V. Mitrofanov, and A. Sergachev, *Sov. At. Energy* **62**, 190 (1987).
- [16] P. Lisowski, A. Gavron, W. Parker, S. Balestrini, A. Carlson, O. Watson, and N. Hill (eds.), *Conference on Nuclear Data for Science and Technology, Juelich*, Vol. MD, 732 (American Institute of Physics, College Park, 1991).
- [17] B. Fursov, E. Baranov, M. Klemyshev, B. Samylin, G. Smirenkin, and Y. Turchin, *At. Energy* **71**, 827 (1992).
- [18] n_TOF Collaboration (TOF Collaboration), *TOF: Proposal for a Neutron Time of Flight Facility, European Collaboratoion for High-Resolution Measurements of Neutron Cross Sections between 1 eV and 250 MeV*, Tech. Rep. CERN-SPSC-99-8. SPSC-P-310 (CERN, Geneva, 1999).
- [19] M. Calviani *et al.*, *Nucl. Instrum. Methods Phys. Res., Sect. A* **594**, 220 (2008).
- [20] A. Koning and D. Rochman, *Nucl. Data Sheets* **113**, 2841 (2012), and references therein.
- [21] M. Diakaki *et al.*, *Proceedings of the 21st Symposium of the Hellenic Nuclear Physics Society* (2012), pp. 81–88.
- [22] M. Mayer, *SIMNRA User's Guide*, Report IPP 9/113 ed. (Max-Planck Institut fur Plasmaphysik, Garching, 1997).
- [23] G. Battistoni, S. Muraro, P. Sala, F. Cerutti, A. Ferrari, S. Roesler, A. Fasso', and J. Ranft, in *Proceedings of the Hadronic Shower Simulation Workshop 2006, Fermilab*, edited by M. Albrow and R. Raja, Vol. 896 (AIP, 2007), pp. 31–49.
- [24] A. Ferrari, P. R. Sala, A. Fasso, and J. Ranft, *FLUKA: A Multi-Particle Transport Code (Program Version 2005)*, Vol. INFN/TC 05/11, SLAC-R-773 (CERN, Geneva, 2005).
- [25] D. Patiris, K. Blekas, and K. Ioannides, *Comput. Phys. Commun.* **177**, 329 (2007).
- [26] MCNPX, *Version 2.5.0, LA-CP-05-0369* (Los Alamos National Laboratory, Los Alamos, 2005).
- [27] U. Abbondanno *et al.*, *Nucl. Instrum. Methods Phys. Res., Sect. A* **538**, 692 (2005).
- [28] D. Karadimos *et al.*, *Nucl. Instrum. Methods Phys. Res., Sect. B* **268**, 2556 (2010).
- [29] F. James, *MINUIT: Function Minimization and Error Analysis Reference Manual (version 94.1)*, Program Library d506 ed. (CERN, Geneva, 1998).
- [30] R. Sarmiento *et al.* (n_TOF Collaboration), *Phys. Rev. C* **84**, 044618 (2011).
- [31] C. Borcea *et al.*, *Nucl. Instrum. Methods Phys. Res., Sect. A* **513**, 524 (2003).
- [32] G. Adeev *et al.*, preprint INR RAS 861/93 (1993).
- [33] I. A. E. Agency, *International Evaluation of Neutron Cross-Section Standards* (STI/PUB/1291, Vienna, Austria, 2007).
- [34] M. Chadwick *et al.*, *Nucl. Data Sheets* **112**, 2887 (2011).
- [35] A. Santamarina *et al.*, *The JEFF-3.1.1 Nuclear Data Library*, NEA No. 6807 (Nuclear Energy Agency, OECD 2009).
- [36] K. Shibata *et al.*, *J. Nucl. Sci. Technol. (Abingdon, UK)* **48**, 1 (2011).
- [37] R. Capote *et al.*, *Nucl. Data Sheets* **110**, 3107 (2009).
- [38] E. S. Soukhovitskii, S. Chiba, J.-Y. Lee, O. Iwamoto, and T. Fukahori, *J. Phys. G* **30**, 905 (2004).
- [39] S. Cohen, F. Plasil, and W. Swiatecki, *Ann. Phys. (NY)* **82**, 557 (1974).
- [40] A. J. Sierk, *Phys. Rev. C* **33**, 2039 (1986).
- [41] <http://www-nds.iaea.org/exfor/exfor.html>
- [42] M. Sin, R. Capote, A. Ventura, M. Herman, and P. Oblozinsky, *Phys. Rev. C* **74**, 014608 (2006).
- [43] M. Herman, R. Capote, B. Carlson, P. Oblozinsky, M. Sin, A. Trkov, H. Wienke, and V. Zerkin, *Nucl. Data Sheets* **108**, 2655 (2007).